Largely enhanced coercivity of cobalt adjacent to straight-stripe mixed-phase bismuth ferrites

Jin Hong Lee,[1,*] Byung-Kweon Jang,[1] Kyung Rok Kang,[1] Dong-Jun Kim,[2] Byong-Guk Park,[2,3] and Chan-Ho Yang[1,3,†]

[1]*Department of Physics, KAIST, Yuseong-gu, Daejeon 34141, Republic of Korea*

[2]*Department of Materials Science and Engineering, KAIST, Yuseong-gu, Daejeon 34141, Republic of Korea*

[3]*KAIST Institute for the NanoCentury, KAIST, Yuseong-gu, Daejeon 34141, Republic of Korea*

(Received 2 August 2017; revised manuscript received 10 February 2018; published 26 March 2018)

Exchange coupling at the interface of an antiferromagnet and a ferromagnet is the major route toward the future magnetoelectric applications of multiferroic bismuth ferrite at room temperature. By using angle-resolved longitudinal magneto-optic Kerr effect microscopy, we have investigated the exchange anisotropy in a ferromagnetic Co layer adjacent to electrically aligned straight-stripe mixed-phase-boundary (MPB) regions of La-5%-doped $BiFeO_3$. We have found that the magnetic easy axis of the exchange-coupled Co layer becomes parallel to the in-plane crystallographic axis nearest to the adjacent MPB elongation axis. The coercive field of the exchange-coupled Co layer along the magnetic easy axis has prominently increased by ∼66 Oe, i.e., 30 times larger than that of a control sample (2.3 Oe), wherein a 5-nm-thick nonmagnetic Ta spacer is placed between the antiferromagnetic and ferromagnetic layers and thus it is intended to have only the shape anisotropy arising from the surface nanostructure of the MPB regions. The finding opens a promising avenue for magnetoelectric applications at room temperature.

DOI: 10.1103/PhysRevB.97.104420

I. INTRODUCTION

The electric-field control of magnetic properties has received much attention as a mechanism for next-generation data processor and information storage by virtue of its potential to reduce the energy dissipation per unit area of devices by more than one or two orders of magnitude [1–5]. In order to realize the electric-field manipulation of magnetic orders, exploring for a room-temperature magnetoelectric multiferroic that displays both magnetic and ferroelectric orders in addition to a strong coupling between the two orders has been a major stream of magnetoelectric materials research [6–10]. Among few room-temperature single-phase multiferroics, $BiFeO_3$ (BFO; $T_C \sim 1100$ K, $T_N \sim 643$ K) [9,11–13] has taken center stage by showing not only a strong ferroelectric polarization ($\sim 90\ \mu C\ cm^{-2}$) [12] but also an electric-field-induced rotation of its antiferromagnetic (AFM) spin axis, $\overleftrightarrow{S}$ [4,9,13–16].

In addition, the discovery of a highly elongated multiferroic tetragonal-like phase (T phase; $T_N \sim 380$ K) and an epitaxially connected structural interface called as mixed-phase boundary (MPB) between the T phase ($c/a \sim 1.23$) and a third polymorph, i.e., S phase ($c/a \sim 1.07$), in compressive-strained BFO thin films has offered another important route toward future magnetoelectric devices [17–19]. However, it has been challenging to utilize the magnetic configurations of BFO polymorphs by themselves due to the lack of a significantly large net magnetization. The limitation is similar to those of the bulk BFO phase and the weakly strained rhombohedral-like phase, for which magnetic exchange coupling in BFO/ferromagnet (BFO/FM) heterostructures has been extensively investigated [4,13,16,20–24]. Besides, only a few reports have considered the local investigation of magnetic exchange coupling in BFO/FM heterostructures [23,24]; such spatially resolved study is essential to reveal the close link between FM and nanosized domains/interfaces of BFO.

Although exotic phenomena such as large electric-field-induced strain [25,26], spontaneous magnetic moment [27], enhanced electronic conduction [28,29], and anisotropic photocurrent [30] have been discovered in the MPB region indicating the unique values of the nanoscale structure, a systematic investigation on the magnetic exchange interaction in the mixed-phase BFO and FM heterostructures for implementation of the multifunctional magnetoelectric devices has remained little explored. In particular, as the parent BFO has curved and broken structures of the MPB regions, the exchange coupling is influenced by many uncontrolled constituents such as the irregular distributions and the end points of the boundaries. In the circumstances, the doping-driven engineered material La-5%-doped $BiFeO_3$ (BLFO) exhibiting a well-ordered straight-stripe MPBs with a uniform boundary density provides useful opportunities to investigate the intrinsic exchange coupling at a quantitative level, to operate the device deterministically and reliably, and to take a big step toward the room-temperature magnetoelectric application.

In this work, we report the exchange-coupling effect between AFM spins in a uniformly aligned MPB region and ferromagnetic spins in mixed-phase BLFO and Co heterostructures. By performing a tip-induced poling via piezoresponse force microscopy (PFM), we prepared four large straight-stripe MPB areas with different MPB elongation axes in BLFO thin films. A thin ferromagnetic Co layer was deposited on the electrically prepared MPB sample and then protected by a Ta capping layer. We determine the exact orientations of the magnetic easy axes of the four prepared regions as well as the as-grown region in

*rifle@kaist.ac.kr
†chyang@kaist.ac.kr

 ©2018 American Physical Society

a spatially resolved way by using angle-resolved longitudinal magneto-optic Kerr effect (MOKE) microscopy and evaluate a MPB-induced large enhancement of the coercive field in the Co layer. To further attest whether the observed anisotropy is due to the magnetic origin, we prepare another specimen by inserting a nonmagnetic Ta spacer between the BLFO layer and the Co layer and examine the magnetic property of the control sample similarly.

II. EXPERIMENTAL METHODS

A. Synthesis of straight-stripe mixed-phase BLFO/Co heterostructure

The whole procedures for materializing exchange-coupled mixed-phase BLFO/FM heterostructures are described in Fig. 1. Mixed-phase BLFO thin films buffered with a $Pr_{0.5}Ca_{0.5}MnO_3$ bottom electrode were synthesized on (001) $LaAlO_3$ substrates by using pulsed laser deposition technique; for detailed growth parameters refer to Ref. [28]. First, two single-box poling experiments are performed on the sample surface using two different slow-scan directions perpendicular to each other, thereby creating four possible MPB axes; for more details, the slow-scan directions are rotated 30° counterclockwise from $[0\bar{1}0]$ or $[\bar{1}00]$ about the [001] axis, respectively. After the PFM poling experiments, in order to form an interface between the aligned MPB regions and the ferromagnetic Co layer where exchange-coupling effect may occur, we deposited a 2.5-nm-thick Co layer capped with a 1-nm-thick Ta layer (in order to prevent the oxidation of the Co layer) by employing ultrahigh-vacuum direct current magnetron sputtering system with a base pressure of 3×10^{-8} Torr and a working pressure of 3 mTorr at room temperature. For a control sample, a 5-nm-thick nonmagnetic Ta spacer was inserted before the Co deposition. The surface quality of all the samples after the metal deposition is comparable to that of the samples before the metal deposition, which ensures that the surface morphology of the straight-stripe mixed-phase BLFO films is well preserved after the whole procedures (see Supplemental Material, Fig. S1 [31]) and infers that the interface quality of all the samples is very high. The goal of this research is to clarify the exchange anisotropy in the ferromagnetic spins adjacent to the four MPB elongation axes (see the bottom of Fig. 1).

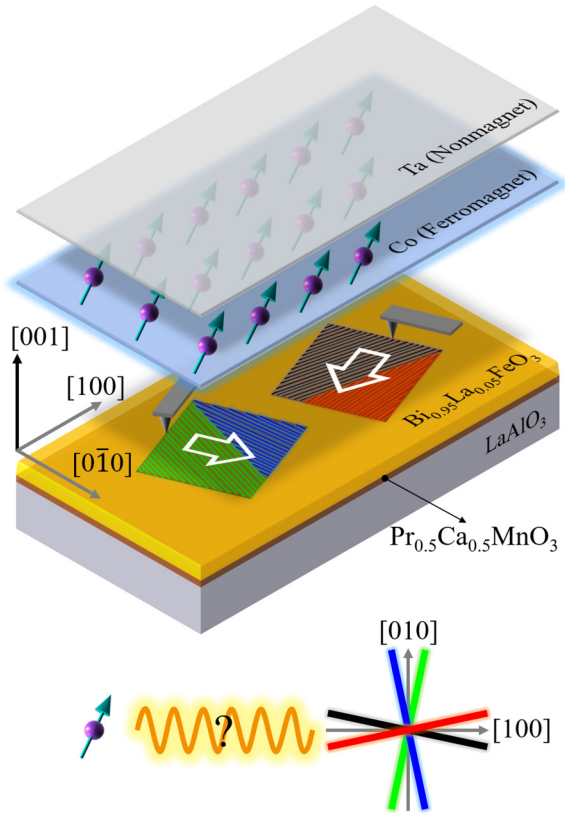

FIG. 1. Schematic diagram for the production process of a straight-stripe mixed-phase BLFO/Co heterostructure. By scanning the BLFO surface with a dc-biased conducting tip, four electrically aligned MPB elongation axes are prepared. Then, a ferromagnetic Co layer with a nonmagnetic Ta capping layer is deposited on the BLFO surface. At the bottom, our question on the exchange coupling between the ferromagnetic spin in the Co layer and the four possible MPB elongation axes in the BLFO layer is visualized.

B. PFM poling and imaging

Electric-field-induced writing of uniformly aligned MPB regions and PFM imaging were performed using Pt-coated Si tips (HQ:NSC35/Pt, MikroMasch) under the combination of Bruker-DI MultiMode V and NanoScope controller V. During the PFM poling experiments, we used a −10-V-biased tip at a velocity of 5 μm s^{-1}.

C. Angle-resolved MOKE microscopy

The local magnetic anisotropy of the Co layer was analyzed through angle-resolved MOKE microscopy. The MOKE microscopy system basically consisted of a polarizing optical microscope (Olympus BX60M), which can visualize magnetic contrast via longitudinal MOKE with maximal spatial resolution of 0.4 μm. In order to measure the longitudinal MOKE [32], the light path was off-centered from the center of the objective lens so the incident light on the sample had a finite incidence angle, ∼20° [33]. The green-color filter of 550 nm was inserted to maximize Kerr signal for the Co layer. The 50-μm×25-μm area was measured with 500× magnification, and the images of the corresponding area were stored in 239 × 119 pixels. In order to enhance the weak signals arising from the very thin Co layer, three steps of image processing were done on the measured images. A set of images for an individual magnetic hysteresis loop was obtained by averaging five images for one data point, and the time for one cycle took ∼51 s in the magnetic field range of −180 to 180 Oe with the magnetic field step of ∼2.8 Oe. The contrast of the stored image was enhanced by subtracting the background image, i.e., the image obtained at a negative saturation field. Finally, 25 sets of images were averaged into a final set of images, and this final set of images was used to display final magnetic hysteresis loops; the linear background signal from the Faraday effect by the applied magnetic field and the constant background signal from regular components of light reflection were also subtracted. In every magnetic hysteresis loop, the MOKE intensity (I_{MOKE}) was normalized to the saturation intensity

(I_S) of a charge-coupled device camera, and one magnetic hysteresis loop is the spatially averaged signal of a selected area. The angle-resolved MOKE microscopy was performed by rotating the sample. For the main sample, $\theta = 0$, 12, 30, 60, 78, 90, 102, 120, 150, 168, 180, 192, 210, 240, 258, 270, 282, 300, 330, and 348° were analyzed. For the control sample, four additional angles, i.e., $\theta = 45$, 135, 225, and 315°, were analyzed. The ±12° from the crystal axes were included in order to check magnetic hysteresis loops along the four MPB elongation axes.

III. RESULTS

A. Electrical aligning of four MPB elongation axes

To determine the MPB elongation axis and the ferroelectric state of electrically written MPB areas, an atomic force microscopy image and an out-of-plane PFM image were measured before the deposition of the ferromagnetic Co layer. Figure 2(a) shows the two single-box-poled MPB regions where the left box marked with the green and blue polygons has the MPB elongation axes almost parallel (±12° off) to the [010] axis but the right box marked with the black and red polygons has the MPB elongation axes almost parallel (±12° off) to the [100] axis. The surface height modulation of each MPB region has the spatial period of 50 ∼ 150 nm (see the two zoomed-in boxes showing a 5× magnified view of the original image). The as-grown area around the two boxes shows the random distribution of the four MPB elongation axes. The out-of-plane PFM image in Fig. 2(b) indicates that both of the two single boxes have upward ferroelectric polarizations in contrast to downward polarizations in the as-grown area. In our system, the out-of-plane polarization switching is indispensable in order to create a large area having only one or two uniformly aligned MPB regions when a voltage-biased scanning tip is used [28]; for reference, the creation of well-aligned MPB regions is also possible by using coplanar top electrodes at slightly increased temperature (70 °C) [34].

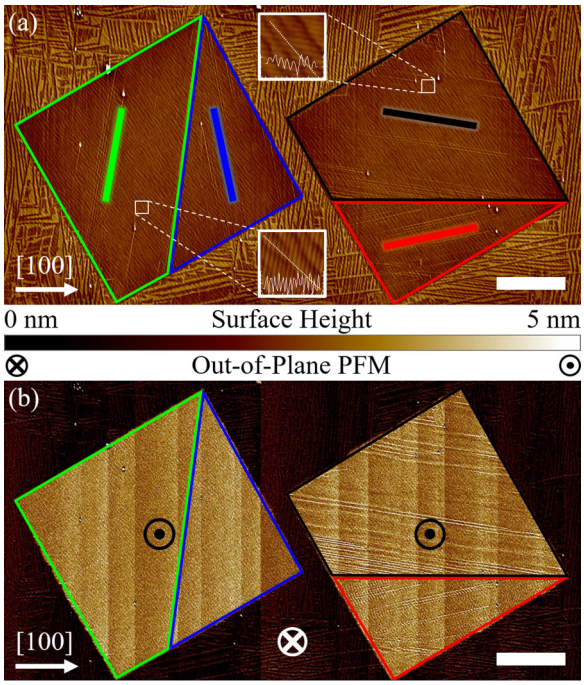

FIG. 2. Electrical aligning of four MPB elongation axes. (a) Atomic force microscope image of two single-box-poled areas including four uniformly aligned MPB elongation axes. The MPB elongation axes within the green and the blue polygons are ±12° off from the [010] crystallographic axis but those within the black and the red polygons are ±12° off from the [100] crystallographic axis. The two white zoomed-in boxes show 5× magnified images of the original image. The line profile along a dotted line in each zoomed-in box shows the height change (∼0.5 nm for peak-to-peak amplitudes) due to the T- and S-phase alternation crossing the periodic MPBs. (b) Out-of-plane PFM image on the same area. Both boxes are in an upward ferroelectric polarization state compared to a downward ferroelectric polarization state in the as-grown area. Scale bars indicate 5 μm.

B. Local magnetic anisotropy imaging by longitudinal MOKE microscopy

The local magnetic anisotropy of selected areas on the Co surface adjacent to the electrically aligned MPB areas can be determined by analyzing local angle-dependent magnetic hysteresis loops using the angle-resolved longitudinal MOKE microscope. Figure 3(a) describes the experimental geometry of our angle-resolved longitudinal MOKE microscopy. Angle-dependent magnetic hysteresis loops are measured by rotating a sample with respect to the fixed magnetic field direction; here, we define an interangle θ between H and the crystallographic [100] direction within the sample surface [Fig. 3(a)]. More detailed information on the angle-resolved longitudinal MOKE microscopy is described in the Experimental Methods section.

Figure 3(b) shows one representative graph including four local magnetic hysteresis loops for the $\theta = 0°(H \parallel [100])$ case where the color of each loop corresponds to that of the MPB elongation axis defined in Fig. 1. For a chosen θ, we first collect a MOKE microscope movie by sweeping an external magnetic field and then the spatially averaged MOKE intensity is extracted from each polygon as a function of the magnetic field. The normalized MOKE intensity (see the Experimental Methods section for more details) of the hysteresis loop is directly proportional to the magnitude of the local magnetization (M) along the applied magnetic-field direction so the obtained hysteresis loops can be regarded as M-H hysteresis loops. Figures 3(c) and 3(d) display two selected still images extracted from a MOKE microscope movie for $\theta = 0°(H \parallel [100])$ when the applied magnetic field was smaller [Fig. 3(c)] or larger [Fig. 3(d)] than the coercive field (H_c) of Co in the right box (the black and the red MPB regions). All the MOKE microscope movies for $\theta = 0°(H \parallel [100])$ and $\theta = 90°(H \parallel [010])$ are provided as supplemental movies [31]. By comparing the changes in the two boxes, we observed that the contrast of the right box changed from black [Fig. 3(c)] to white [Fig. 3(d)] but that of the left box did not change much and stayed a gray color. In addition, the as-grown areas with black contrast also changed to white contrast. Throughout the repeated magnetic-field sweeps, we found that the contrast of the right box changes abruptly near the coercive field but that of the left box changes continuously.

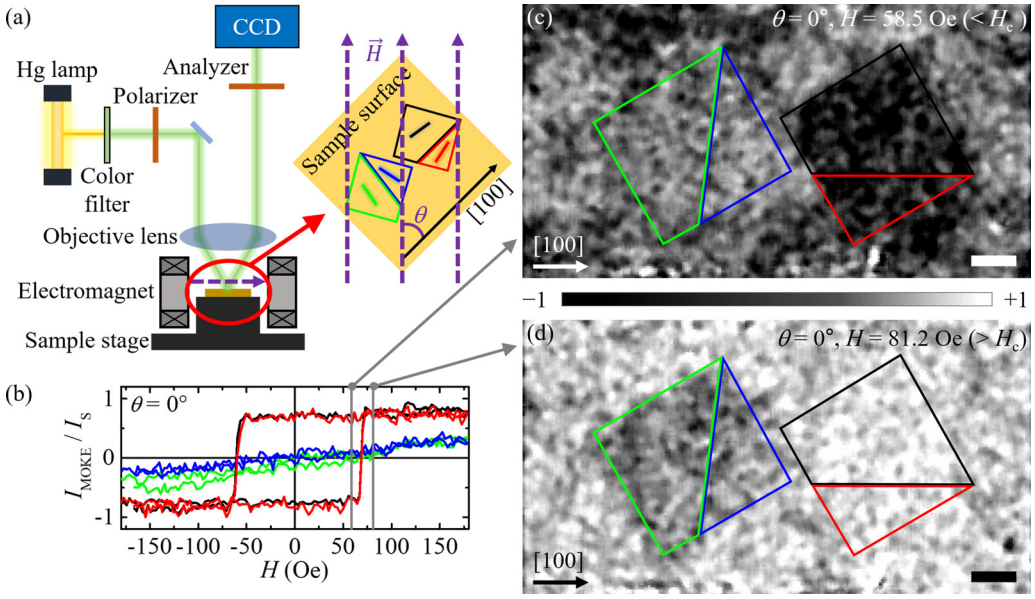

FIG. 3. Angle-resolved longitudinal MOKE microscopy. (a) Schematic diagram of an angle-resolved longitudinal MOKE microscopy. A linearly polarized light is reflected from the Co surface and it passes through an analyzer. The purple vector indicates the direction of an external magnetic field, and the in-plane angle θ from the [100] crystallographic axis is described. (b) Four local magnetic hysteresis loops of the Co layer adjacent to the electrically written MPB areas for the $\theta = 0°$($H \parallel$ [100]) case. The selected MOKE microscope images corresponding to the hysteresis loops in (b) when the applied magnetic field is below (c) and above (d) the coercive field, H_c. The scale bars indicate 5 μm.

In consideration of the MPB elongation axis of each region, the result infers that the easy axis of the ferromagnetic spins in the Co layer becomes more parallel to the MPB elongation axis.

C. Angle-resolved longitudinal MOKE microscopy

In order to confirm the detailed relation between the magnetic easy axis of Co and the MPB elongation axis of each region, angle-dependent magnetic hysteresis loops were measured (see Fig. S2 [31]). In Fig. 4(a), four sets of angle-dependent M-H hysteresis loops from each MPB region are presented where the color of each loop corresponds to the selected angle ($\theta = 0, 12, 30, 60, 78,$ and $90°$; see the schematic in the center of Fig. 4). When the angle approaches 90°, the magnetic hysteresis loops from the green and the blue MPB regions become more square loops but those from the black and the red MPB regions become almost linear lines through the origin. Such trend is reversed when the angle approaches 0°. Another important consequence is that although the MPB elongation axes of the green and the blue MPB regions (or the MPB elongation axes of the black and the red MPB regions) differ by 24°, the hysteresis loops from the two regions overlap each other. In other words, the MPB elongation axes within one PFM-poled box induce the same magnetic anisotropy in the adjacent ferromagnetic layer.

D. Comparison with the control sample

The observed magnetic anisotropy in the Co layer could come from the periodic surface roughness of the MPB regions, the exchange-coupling effect between Co and BLFO, or from both so we carried out the same experiments on the control sample which has a 5-nm-thick nonmagnetic Ta spacer between Co and BLFO layers. The smooth nonmagnetic Ta spacer kept and delivered the surface nanostructure of the MPB regions to the upper Co layer but removed the direct contact of Co and BLFO after the deposition so the structural effect (or shape anisotropy) of the MPB regions was effectively isolated from the exchange coupling effect (see the Experimental Methods section and Fig. S1 [31] representing a high-quality surface of the control sample). Figure 4(b) is the result for the control sample (see also Fig. S3 [31]). The coercive field of the control sample significantly decreased by more than one order of magnitude ($H_C = 2.3 \pm 0.3$ Oe; see the horizontal scale for the magnetic field) in comparison with that of the main sample along the magnetic easy axis ($H_C = 68 \pm 6$ Oe). In other words, the coercive field of the ferromagnetic layer along the magnetic easy axis can increase by ~66 Oe due to its exchange coupling with the MPB regions. Therefore, we can reasonably conclude that the observed magnetic anisotropy in the main sample is mostly caused by the exchange-coupling effect at the interface between Co and MPB, i.e., exchange anisotropy. Moreover, we note that the exchange bias [35] of our system, i.e., the horizontal shift of a hysteresis loop, is very small (a few Oe) and does not show any clear correlation with MPB elongation axes as shown in Figs. S4 and S5 [31].

E. Magnetic easy- and hard axes in heterostructures

Figures 5(a)–5(c) show polar plots displaying the squareness ratios of hysteresis loops (remanent magnetization M_R over saturation magnetization M_S) as a function of θ (Ref. [36]), which provide us an easier view of the magnetic anisotropy in each MPB region and the as-grown region. The squareness ratio becomes unity when the shape of a hysteresis loop is exact square but zero when the remanent magnetization

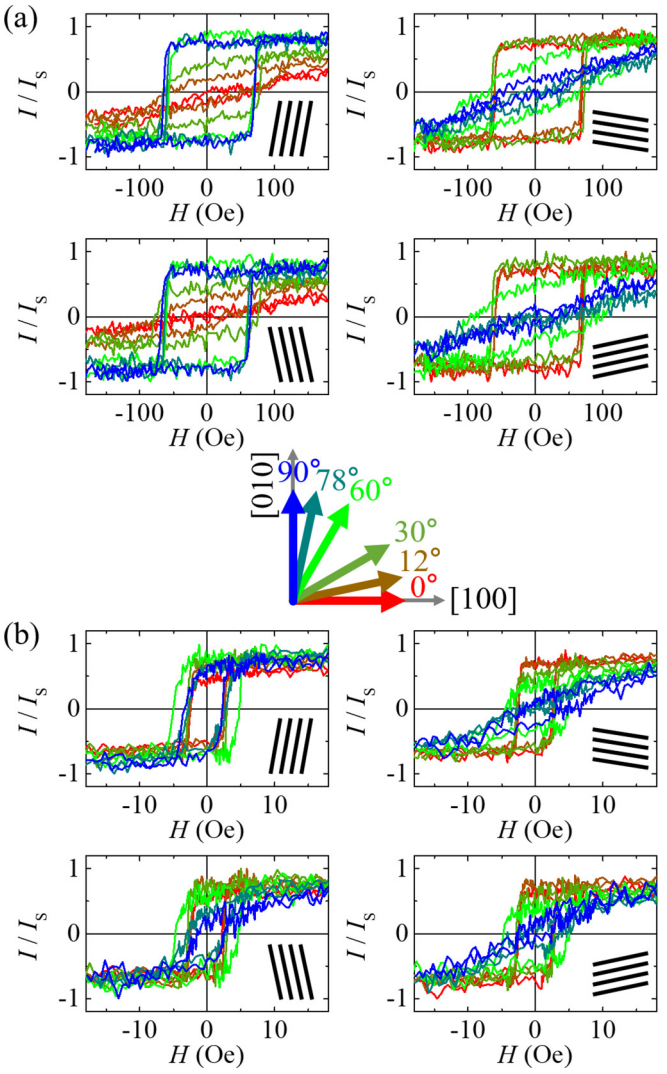

FIG. 4. Four sets of angle-dependent magnetic hysteresis loops from the four electrically written MPB regions for (a) the main sample and (b) the control sample are shown, where the color of each loop corresponds to the selected angle (θ = 0, 12, 30, 60, 78, and 90°; see the schematic in the center). In the lower right corner of each graph, the MPB elongation axis is described.

is zero; thus, it is a good indicator for the magnetic easy axis. In Figs. 5(a) and 5(b), it is clearly shown that dumbbell-like curves where the major axes of the green and the blue curves (parallel to the [010] axis) are perpendicular to those of the black and the red curves (parallel to the [100] axis). Therefore, in the main sample, there exists the almost parallel relation between the magnetic easy axis of the Co layer and the MPB elongation axis of the BLFO layer. However, as shown in Fig. 5(c), the as-grown region does not show any noticeable magnetic anisotropy due to randomly aligned MPB elongation axes. Figure 5(d) summarizes the determined magnetic easy axis of Co on each MPB region. The same analysis done on the control sample is provided in Fig. 6. Unexpectedly, all the regions in the control sample show a uniaxial magnetic anisotropy along the [100] axis. If the coercive field of the non-exchange-coupled Co layer in the control sample becomes very small, any other factors than the structural effect of the

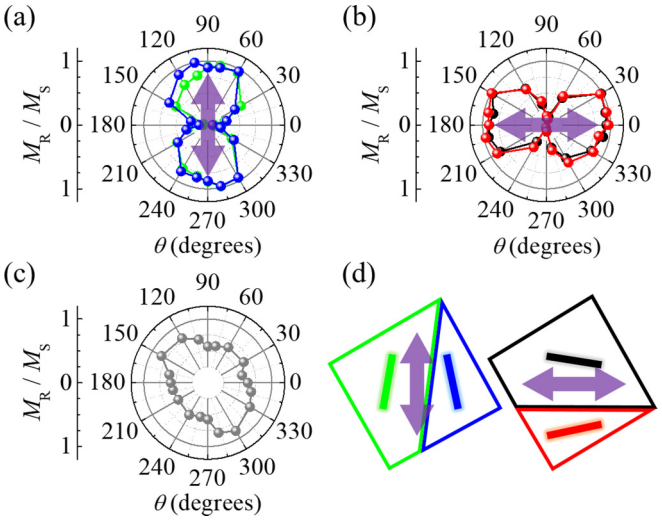

FIG. 5. Determination of magnetic easy- and hard axes in MPB/Co heterostructures. Polar plots for the squareness ratio of (a) the green/blue MPB regions inside the left box, (b) the black/red MPB regions inside the right box, and (c) the as-grown region in the main sample (without a nonmagnetic Ta spacer). The color of each symbol and curve corresponds to the electrically aligned MPB region with the same color. The determined magnetic easy axis of each MPB region is expressed inside each polar plot. (d) Schematic diagram summarizing the magnetic easy axis of the MPB regions.

MPB regions may compete to create the magnetic anisotropy of the control sample. We suspect that twin boundaries of the rhombohedral $LaAlO_3$ substrate, i.e., parallel to the [010] axis in this sample as shown in Fig. 7, can be the main factor breaking the in-plane symmetry.

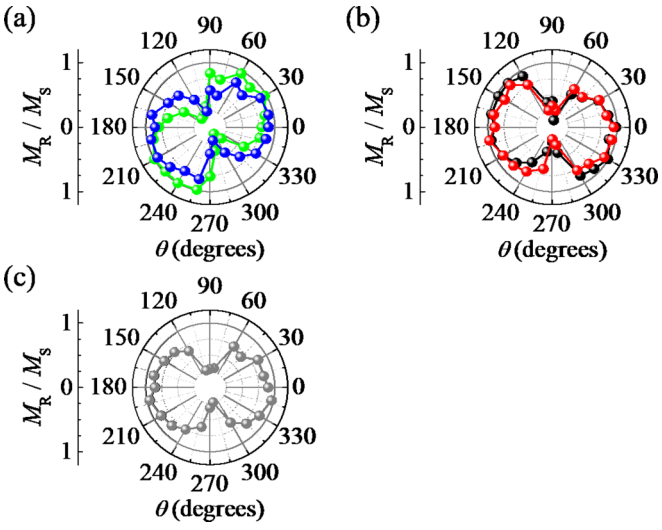

FIG. 6. Determination of magnetic easy- and hard axes in the control sample (the non-exchange-coupled system). Polar plots for the squareness ratio of (a) the green/blue MPB regions inside the left box, (b) the black/red MPB regions inside the right box, and (c) the as-grown region in the control sample (with a nonmagnetic Ta spacer). The color of each symbol and curve corresponds to the electrically aligned MPB region with the same color.

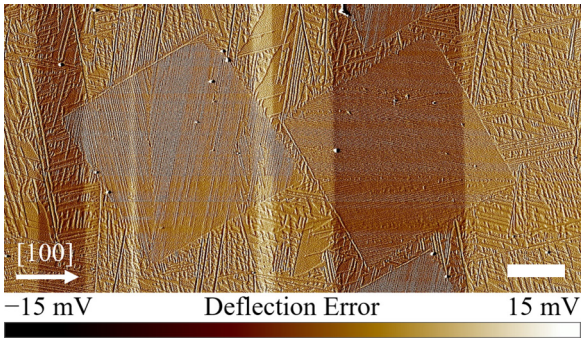

FIG. 7. Deflection error image of the control sample where the image contrast is proportional to the surface slope. The long-range twin structure of the rhombohedral $LaAlO_3$ substrate is visible, and the twin boundaries are parallel to the [010] axis. Scale bar indicates 5 μm.

IV. DISCUSSION

The microscopic origin of the observed exchange anisotropy in the mixed-phase BLFO/Co heterostructure can be discussed from two points of view: (1) the AFM structure of the MPB region [37] and (2) the enhanced spontaneous magnetization of *S* phase in the MPB region [27]. Regarding the first scenario, Lee *et al.* [37] showed that the AFM axis of one MPB region is parallel to the crystallographic axis that is almost perpendicular to the MPB elongation axis. Since our BLFO samples possess an atomically smooth surface, the surface of BLFO can be regarded as a perfectly compensated AFM surface. It has been well understood that for a compensated AFM/ferromagnetic interface, the interfacial exchange coupling induces perpendicular alignment between AFM and ferromagnetic spins [38,39], so this scenario agrees with the observed exchange anisotropy that the magnetic easy axis of the ferromagnetic Co layer becomes parallel to the crystallographic axis nearest to the adjacent MPB elongation axis. Additionally, the observed negligible exchange bias can be well explained in the consideration of the compensated AFM surface [40,41]. In the second scenario, as reported in the work of He *et al.* [27], the enhanced spontaneous magnetization of *S* phase in a MPB region which aligns parallel to the MPB elongation axis can be a driving force of the parallel alignment between the ferromagnetic layer and the adjacent BFO layer. Although the exact origin of the enhanced spontaneous magnetization of *S* phase is still elusive, the direction of the magnetization is one possible direction of canted spin moments due to the Dzyaloshinskii-Moriya interaction within the AFM spin structure of the first scenario. Therefore, both points of view mutually support our observation on the exchange anisotropy in the mixed-phase BLFO/Co heterostructures.

Although our observation has been well understood within the context of magnetic exchange anisotropy, we would like to address other possible scenarios which can also contribute to the observed magnetic anisotropy through the FM/ferroelectric interfacial coupling. By synthesizing a bilayer of ferroelectric $PbZr_{0.2}Ti_{0.8}O_3$ and colossal magnetoresistive $La_{0.8}Sr_{0.2}MnO_3$, Molegraaf *et al.* [42] reported that the magnetization of a magnetic layer can be modulated by switching the electric polarization of an adjacent ferroelectric layer, i.e., field-effect doping. Lahtinen *et al.* [43] demonstrated the electric-field control of magnetic domains via strain transfer in a $CoFe/BaTiO_3$ heterostructure. In a $FeRh/BaTiO_3$ system, the electric-field-induced transition between antiferromagnetic and ferromagnetic order was observed by Cherifi *et al.* [44]. The relevance of these interfacial mechanisms remains an interesting future study.

V. CONCLUSIONS

In summary, we visualized magnetic domain switching of a ferromagnetic Co layer on the electrically patterned multiferroic states by angle-resolved longitudinal MOKE microscopy. We confirmed that the ferromagnetic spins align parallel to the in-plane crystallographic ⟨100⟩ axis nearest to the local MPB elongation axis of BLFO. Furthermore, we quantified that the coercive field of the ferromagnetic Co layer was increased by ∼66 Oe as a result of the exchange coupling between Co and the straight-stripe MPB region while the exchange bias was negligible. Our experimental demonstration suggests a possibility of the strong magnetic exchange interaction inherent in the MPB region.

ACKNOWLEDGMENTS

We especially thank Sung-Chul Shin from Department of Physics at KAIST for allowing us to use the MOKE microscope in his laboratory. This work was supported by the National Research Foundation (NRF) Grant funded by the Korean Government via the Center for Lattice Defectronics (Grant No. NRF-2017R1A3B1023686) and the Center for Quantum Coherence in Condensed Matter (Grant No. 2016R1A5A1008184). B.-G.P. acknowledges financial support from the DGIST R&D Program (Grant No. 17-BT-02).

J.H.L. and B.-K.J. contributed equally to this work.

[1] S. Fusil, V. Garcia, A. Barthélémy, and M. Bibes, Annu. Rev. Mater. Res. **44**, 91 (2014).
[2] F. Matsukura, Y. Tokura, and H. Ohno, Nat. Nanotechnol. **10**, 209 (2015).
[3] C. A. F. Vaz, J. Phys.: Condens. Matter **24**, 333201 (2012).
[4] J. T. Heron, D. G. Schlom, and R. Ramesh, Appl. Phys. Rev. **1**, 021303 (2014).
[5] D. Chiba, Front. Phys. **3**, 83 (2015).
[6] M. Fiebig, J. Phys. D: Appl. Phys. **38**, R123 (2005).
[7] W. Eerenstein, N. D. Mathur, and J. F. Scott, Nature (London) **442**, 759 (2006).
[8] S.-W. Cheong and M. Mostovoy, Nat. Mater. **6**, 13 (2007).
[9] R. Ramesh and N. A. Spaldin, Nat. Mater. **6**, 21 (2007).
[10] Y. Tokura and S. Seki, Adv. Mater. **22**, 1554 (2010).
[11] F. Kubel and H. Schmid, Acta Crystallogr., Sect. B: Struct. Sci. **46**, 698 (1990).
[12] D. Lebeugle, D. Colson, A. Forget, and M. Viret, Appl. Phys. Lett. **91**, 022907 (2007).

[13] J. T. Heron, J. L. Bosse, Q. He, Y. Gao, M. Trassin, L. Ye, J. D. Clarkson, C. Wang, J. Liu, S. Salahuddin, D. C. Ralph, D. G. Schlom, J. Íñiquez, B. D. Huey, and R. Ramesh, Nature (London) **516**, 370 (2014).
[14] C. Ederer and N. A. Spaldin, Phys. Rev. B **71**, 060401(R) (2005).
[15] T. Zhao, A. Scholl, F. Zavaliche, K. Lee, M. Barry, A. Doran, M. P. Cruz, Y. H. Chu, C. Ederer, N. A. Spaldin, R. R. Das, D. M. Kim, S. H. Baek, C. B. Eom, and R. Ramesh, Nat. Mater. **5**, 823 (2006).
[16] Y.-H. Chu, L. W. Martin, M. B. Holcomb, M. Gajek, S.-J. Han, Q. He, N. Balke, C.-H. Yang, D. Lee, W. Hu, Q. Zhan, P.-L. Yang, A. Fraile-Rodríguez, A. Scholl, S. X. Wang, and R. Ramesh, Nat. Mater. **7**, 478 (2008).
[17] B.-K. Jang, J. H. Lee, K. Chu, P. Sharma, G.-Y. Kim, K.-T. Ko, K.-E. Kim, Y.-J. Kim, K. Kang, H.-B. Jang, H. Jang, M. H. Jung, K. Song, T. Y. Koo, S.-Y. Choi, J. Seidel, Y. H. Jeong, H. Ohldag, J.-S. Lee, and C.-H. Yang, Nat. Phys. **13**, 189 (2017).
[18] R. J. Zeches, M. D. Rossell, J. X. Zhang, A. J. Hatt, Q. He, C.-H. Yang, A. Kumar, C. H. Wang, A. Melville, C. Adamo, G. Sheng, Y.-H. Chu, J. F. Ihlefeld, R. Erni, C. Ederer, V. Gopalan, L. Q. Chen, D. G. Schlom, N. A. Spaldin, L. W. Martin, and R. Ramesh, Science **326**, 977 (2009).
[19] C. Beekman, W. Siemons, T. Z. Ward, M. Chi, J. Howe, M. D. Biegalski, N. Balke, P. Maksymovych, A. K. Farrar, J. B. Romero, P. Gao, X. Q. Pan, D. A. Tenne, and H. M. Christen, Adv. Mater. **25**, 5561 (2013).
[20] H. Béa, M. Bibes, F. Ott, B. Dupé, X.-H. Zhu, S. Petit, S. Fusil, C. Deranlot, K. Bouzehouane, and A. Barthélémy, Phys. Rev. Lett. **100**, 017204 (2008).
[21] D. Lebeugle, A. Mougin, M. Viret, D. Colson, and L. Ranno, Phys. Rev. Lett. **103**, 257601 (2009).
[22] J.-M. Hu, L.-Q. Chen, and C.-W. Nan, Adv. Mater. **28**, 15 (2016).
[23] M. Trassin, J. D. Clarkson, S. R. Bowden, J. Liu, J. T. Heron, R. J. Paull, E. Arenholz, D. T. Pierce, and J. Unguris, Phys. Rev. B **87**, 134426 (2013).
[24] L. You, B. Wang, X. Zou, Z. S. Lim, Y. Zhou, H. Ding, L. Chen, and J. Wang, Phys. Rev. B **88**, 184426 (2013).
[25] J. X. Zhang, B. Xiang, Q. He, J. Seidel, R. J. Zeches, P. Yu, S. Y. Yang, C. H. Wang, Y.-H. Chu, L. W. Martin, A. M. Minor, and R. Ramesh, Nat. Nanotechnol. **6**, 98 (2011).
[26] A. R. Damodaran, C.-W. Liang, Q. He, C.-Y. Peng, L. Chang, Y.-H. Chu, and L. W. Martin, Adv. Mater. **23**, 3170 (2011).
[27] Q. He, Y.-H. Chu, J. T. Heron, S. Y. Yang, W. I. Liang, C. Y. Kuo, H. J. Lin, P. Yu, C. W. Liang, R. J. Zeches, W. C. Kuo, J. Y. Juang, C. T. Chen, E. Arenholz, A. Scholl, and R. Ramesh, Nat. Commun. **2**, 225 (2011).
[28] K.-E. Kim, B.-K. Jang, Y. Heo, J. H. Lee, M. Jeong, J. Y. Lee, J. Seidel, and C.-H. Yang, NPG Asia Mater. **6**, e81 (2014).
[29] J. Seidel, M. Trassin, Y. Zhang, P. Maksymovych, T. Uhlig, P. Milde, D. Köhler, A. P. Baddorf, S. V. Kalinin, L. M. Eng, X. Pan, and R. Ramesh, Adv. Mater. **26**, 4376 (2014).
[30] K. Chu, B.-K. Jang, J. H. Sung, Y. A. Shin, E.-S. Lee, K. Song, J. H. Lee, C.-S. Woo, S. J. Kim, S.-Y. Choi, T. Y. Koo, Y.-H. Kim, S.-H. Oh, M.-H. Jo, and C.-H. Yang, Nat. Nanotechnol. **10**, 972 (2015).
[31] See Supplemental Material at http://link.aps.org/supplemental/10.1103/PhysRevB.97.104420 for the surface morphology of the control sample, the angle-dependent magnetic hysteresis loops of the main and the control sample, the angle-dependent exchange bias of the main and the control sample, and the MOKE microscope movies for $\theta = 0$ and 90°.
[32] A. Hubert and R. Schäfer, *Magnetic Domains: The Analysis of Magnetic Microstructures* (Springer, Berlin, 1998).
[33] D.-H. Kim, S.-B. Choe, and S.-C. Shin, Phys. Rev. Lett. **90**, 087203 (2003).
[34] J. Zhou, M. Trassin, Q. He, N. Tamura, M. Kunz, C. Cheng, J. Zhang, W.-I. Liang, J. Seidel, C.-L. Hsin, and J. Wu, J. Appl. Phys. **112**, 064102 (2012).
[35] J. Nogués and I. K. Schuller, J. Magn. Magn. Mater. **192**, 203 (1999).
[36] Q. Wu, W. He, H.-L. Liu, J. Ye, X.-Q. Zhang, H.-T. Yang, Z.-Y. Chen, and Z.-H. Chen, Sci. Rep. **3**, 1547 (2013).
[37] J. H. Lee, K.-E. Kim, B.-K. Jang, A. A. Ünal, S. Valencia, F. Kronast, K.-T. Ko, S. Kowarik, J. Seidel, and C.-H. Yang, Phys. Rev. B **96**, 064402 (2017).
[38] N. C. Koon, Phys. Rev. Lett. **78**, 4865 (1997).
[39] M. Finazzi, Phys. Rev. B **69**, 064405 (2004).
[40] T. C. Schulthess and W. H. Butler, Phys. Rev. Lett. **81**, 4516 (1998).
[41] J. Nogués, J. Sort, V. Langlais, V. Skumryev, S. Suriñach, J. S. Muñoz, and M. D. Baró, Phys. Rep. **422**, 65 (2005).
[42] H. J. A. Molegraaf, J. Hoffman, C. A. F. Vaz, S. Gariglio, D. van der Marel, C. H. Ahn, and J.-M. Triscone, Adv. Mater. **21**, 3470 (2009).
[43] T. H. E. Lahtinen, J. O. Tuomi, and S. van Dijken, Adv. Mater. **23**, 3187 (2011).
[44] R. O. Cherifi, V. Ivanovskaya, L. C. Phillips, A. Zobelli, I. C. Infante, E. Jacquet, V. Garcia, S. Fusil, P. R. Briddon, N. Guiblin, A. Mougin, A. A. Ünal, F. Kronast, S. Valencia, B. Dkhil, A. Barthélémy, and M. Bibes, Nat. Mater. **13**, 345 (2014).